Nanoscale

PAPER

View Article Online
View Journal | View Issue

Cite this: *Nanoscale*, 2015, **7**, 2352

Self-assembly of metal atoms (Na, K, Ca) on graphene†

Jian Zhou,[a] Shunhong Zhang,[b] Qian Wang,[b,c,a] Yoshiyuki Kawazoe[d] and Puru Jena*[a]

Received 10th October 2014,
Accepted 17th December 2014

DOI: 10.1039/c4nr05990e

www.rsc.org/nanoscale

A thorough search of the distribution pattern of Na, K, and Ca atoms on graphene surface, carried out using a synergistic combination of density functional theory and particle swarm optimization algorithm, yielded some unusual results. The equilibrium distribution is concentration and metal dependent; the metal atoms distribute uniformly when their coverage ratio M : C (M = Na, K, Ca) is 1 : 6, but Na and Ca atoms self-assemble to form parallel quasi-one-dimensional chains when their coverage is reduced to 1 : 8. At the higher concentration (M : C = 1 : 6), electron–phonon coupling calculations further show that the NaC_6 is a superconductor with critical temperature of 5.8 K, which is the highest value among all the stable alkali or alkaline-earth metal decorated monolayer graphene systems studied to-date. At the lower concentration (M : C = 1 : 8) and depending on metal species, well-aligned atomic metal chains interact with graphene with varying intensity, making it possible to achieve either rigid or non-rigid band doping in graphene.

I. Introduction

Functionalization of graphene sheet[1] has become a topic of great current interest due to its potential for many technological applications. For example, decoration of graphene surface with hydrogen, oxygen, and fluorine atoms can be used to modulate its electronic properties, such as band gap, electron mobility, and optical absorption.[2–4] Similarly, alkali metal (AM) and alkaline-earth metal (AEM) atoms adsorbed graphene sheets are considered as potential devices for ion batteries, hydrogen storage materials, and superconductors.[5–8] Unlike nonmetal atoms that can perturb the atomic structure of graphene, decoration by AM and AEM has little effect on its geometric structure.[7] The main role of these metal atoms is to donate electrons to the graphene sheet, which makes it n-doped.

The distribution patterns of AM and AEM atoms on the graphene vary with respect to their coverage. When the concentration is dilute, the metal atoms prefer to disperse on the graphene surface. On the contrary, when concentration of metal atoms exceeds a certain critical value, they tend to form compact patterns. What remains elusive is the distribution pattern at intermediate concentrations. Due to the complexity of the energy landscape of the graphene surface and the interaction between deposited metal atoms, predicting the AM or AEM adsorption pattern at intermediate concentration is challenging. Knowing the exact adsorption pattern of AM or AEM on graphene at intermediate concentration will facilitate the exploration of their potential for catalysis and other technological applications.

Using first-principles density functional theory (DFT) combined with particle swarm optimization (PSO) algorithm, we have carried out a systematic global search of deposition pattern of Na, K, and Ca on a single graphene layer. We show that when the coverage ratio M : C = 1 : 6 (M = Na, K, and Ca), all three metal atoms prefer to distribute uniformly. This is in contrast to Li atoms which were found to cluster due to their small size.[9] In addition, we find that NaC_6 monolayer is superconducting with a critical temperature T_c = 5.8 K. KC_6 monolayer, on the other hand, is not superconducting. When the M : C ratio is lowered to 1 : 8, K atoms still form a uniform deposition pattern, while the smaller Na and Ca atoms self-assemble to form quasi-one-dimensional (quasi-1D) metallic chains. Studies of quasi-1D systems both experimentally and theoretically[10] are attracting considerable attention. On one hand, due to their high anisotropy and restricted dimensionality, quasi-1D systems are considered as elemental building blocks for future electronic devices.[11] On the other hand, due to the fundamental difference between the electronic conduc-

[a]*Department of Physics, Virginia Commonwealth University, Richmond, VA 23284, USA. E-mail: pjena@vcu.edu*
[b]*HEDPS, Center for Applied Physics and Technology, College of Engineering, Peking University, Beijing 100871, China*
[c]*Department of Materials Science and Engineering, College of Engineering, Peking University, Beijing 100871, China*
[d]*Institute for Material Research, Tohoku University, Sendai, 980-8577, Japan*

†Electronic supplementary information (ESI) available: Phonon dispersion of free standing Na chain, band structure of 'empty' Ca chain, and work function variation of MC_x with respect to the concentration $1/x$. See DOI: 10.1039/c4nr05990e

tivity of 1D and 2D/3D metallic conductors, understanding the behavior of highly confined 1D electron system (described by Luttinger liquid model rather than conventional Landau's Fermi liquid quasiparticle theory) is interesting and challenging, both theoretically and experimentally.[12] It is, therefore, important to fabricate a system capable of supporting a Luttinger liquid state.[13] One way to realize this is to find a way to grow thin metallic nanowires or nanochains on a surface. Previously, quasi-1D AM or AEM chains were observed on semiconducting and transition metal surfaces where the metal atoms and the substrate are chemically bonded and strongly hybridized.[14–16] In this case, the electronic behavior of these quasi-1D metal atom chains are not genuinely 1D, and mostly they even exhibit dielectric behavior.[17] Here, we show that both the Na and Ca chains on graphene are metallic. Furthermore, the Na and C hybridize weakly around the Fermi level. As a result, the Na chain can retain its essential free standing physical properties and provides an added opportunity to study the behavior of 1D electron systems.

II. Computational methods and models

Our calculations are based on first-principles density functional theory (DFT) with the generalized gradient approximation (GGA) for exchange–correlation functional proposed by Perdew, Burke, and Ernzerhof (PBE)[18] and implemented in the Vienna *ab initio* Simulation Package (VASP).[19] The projector augmented wave (PAW) method with 400 eV energy cut-off for plane-wave basis sets are applied.[20] In order to simulate the 2D systems, we use periodic boundary condition with a vacuum space of 12 Å along the non-periodic z direction. The reciprocal space is represented by the Monkhorst–Pack special k point scheme[21] with density of grid points along x and y directions of $2\pi \times 0.02$ Å^{-1}. Conjugated gradient scheme is adopted to relax the geometric structures without any symmetric constraint. Grimme's method[22] is used to incorporate van der Waals interaction corrections between the metal atoms and the graphene substrate. Convergence criteria for total energy and Hellmann–Feynman force are set to be 1×10^{-4} eV and 0.01 eV Å^{-1}, respectively. The dynamic stability and electron–phonon coupling (EPC) of the NaC_6 and KC_6 are calculated using the Quantum-ESPRESSO package[23] and norm-conserving pseudopotentials. Phonon frequencies are calculated using the density functional linear-response method.[24] Based on convergence tests; we adopt a kinetic energy cutoff of 60 Ry and $(96 \times 96 \times 1)$ k-point mesh in the first Brillouin zone. EPC matrix elements are computed on a $(6 \times 6 \times 1)$ q-mesh.

In order to search for the globally optimal deposition pattern of metal atoms on graphene, we recall that the adsorption of AM and AEM has little effect on the geometric structure of graphene,[7] to reduce the computational cost we fix the substrate C atoms and allow the adatoms to move progressively towards the optimal adsorption site. Different kinds of supercells were also used to minimize the constraints of the periodic boundary condition. For M : C = 1 : 6, we adopt hexagonal (3×3), $\left(2\sqrt{3} \times 2\sqrt{3}\right)$ $R30°$, $\left(\sqrt{21} \times \sqrt{21}\right)$ $R10.9°$, and $\left(3\sqrt{3} \times 3\sqrt{3}\right)$ $R30°$ supercells, which accommodate M_3C_{18}, M_4C_{24}, M_7C_{42}, and M_9C_{54} moieties, respectively. We also use four rectangular supercells, accommodating M_2C_{12}, M_4C_{24}, M_6C_{36}, and M_8C_{48} moieties. For M : C = 1 : 8, we apply hexagonal $\left(2\sqrt{3} \times 2\sqrt{3}\right)$ $R30°$, (4×4), and $\left(2\sqrt{7} \times 2\sqrt{7}\right)$ $R19.1°$ supercells to accommodate M_3C_{24}, M_4C_{32}, and M_7C_{56} moieties, respectively. Rectangular supercells of M_2C_{16}, M_3C_{24}, M_4C_{32}, M_5C_{40}, and M_6C_{48} are also used to study the M : C = 1 : 8 concentration. In each supercell, we randomly generate 20 different metal adsorption patterns which are considered as the initial generation. Each pattern (also called a particle) evolves following an iterative scheme, namely, it first finds the nearest local minimum through standard DFT structural optimization, and in the next generation it surmounts energy barriers to approach lower-lying minima according to the particle swarm optimization (PSO) algorithm.[25] The PSO algorithm has been well tested to predict the geometric structures of 0D clusters,[26] 2D sheets,[27] 3D crystals,[28] and surface reconstructions.[29] We refer to our scheme as partial PSO (PPSO) method as only the adsorbed atoms in our simulated system evolves according to the PSO algorithm. In the PPSO algorithm, the position of each particle x is evolved as,

$$x_i^{t+1} = x_i^t + v_i^{t+1}, \quad (1)$$

where t refers to the generation step, i is the individual particle index (i = 1, 2, ..., 20), and v is the velocity. For each particle i, we collect the best (lowest energy) position that has been reached, and denote it as pbest_i^t. The best position of all the particles that have been found up to now is called "globally best" and denoted as gbest^t. Then the evolving velocity of each particle i can be written as

$$v_i^{t+1} = \omega v_i^t + c_1 r_1 (\mathrm{pbest}_i^t - x_i^t) + c_2 r_2 (\mathrm{gbest}^t - x_i^t), \quad (2)$$

where r_1 and r_2 are random numbers in the range [0, 1]. The parameter ω linearly decreases from 0.9 to 0.4 during iteration.[25,30] The values of c_1 and c_2 are selected to be 2, which are found to efficiently lead to the global minimum.[25,30] After several generations, we find that the gbest^t structure remains unchanged, suggesting that the search process converges to an optimal state. This is considered to be a candidate ground state in that supercell. These energetically low-lying candidates are then fully relaxed to eliminate the effects of lattice constraint on the energy sequence during the structural search. We find that the small relaxation of the graphene substrate has no effect on the relative stability of different isomers. After that, by comparing the relative stability through total energies per formula unit (denoted as E/f.u.) of all the candidate ground states, we obtain the globally optimal desorption pattern.

III. Results

After our PPSO search, we find that for M : C = 1 : 6 (M = Na, K, Ca), the systems converge to a uniform distribution pattern

possessing plane symmetry group of *P6m*. This behavior is in contrast with the case of Li on graphene where Li atoms prefer to form isolated islands.[9] This is because the radii of Na (1.90 Å), Ca (1.94 Å), and K (2.43 Å) are larger than that of the Li (1.67 Å).[31]

Recalling that the CaC_6-*P6m* monolayer is superconducting with a critical temperature T_c = 1.4 K,[5] we explored the possibility of phonon mediated superconductivity of the NaC_6-*P6m* and KC_6-*P6m* monolayers by calculating the phonon dispersion, Eliashberg function $\alpha^2F(\omega)$, and EPC parameter $\lambda(\omega)$.[32] No imaginary frequencies were found in the phonon spectra of NaC_6-*P6m*, (Fig. 1a), confirming that it is dynamically stable. As shown in Fig. 1b, emergence of several sharp peaks explicitly suggest strong coupling between electrons on the Fermi surfaces and phonon modes in both low and high frequency regions, and the total EPC parameter, λ = 1.46, and the logarithmic frequency average ω_{log} is 54.47 K. By using Allen–Dynes modified McMillan equation[33]

$$T_c = \frac{\hbar\omega_{log}}{1.2k_B}\exp\left[\frac{-1.04(1+\lambda)}{\lambda-\mu^*(1+0.62\lambda)}\right] \quad (3)$$

which has been widely used to estimate the T_c of BCS superconductors and the typical value of 0.115 for the effective Coulomb repulsion parameter μ^*, we obtain T_c of NaC_6-*P6m* to be 5.8 K. This value is larger than that of the CaC_6-*P6m* monolayer (1.4 K).[5] The KC_6-*P6m* is not found to be a superconductor. These results are consistent with the fact that smaller distance between the metal layer and the graphene can induce larger EPC, and hence higher T_c.[5] Noting that the LiC_6-*P6m* is not the energetically most stable configuration,[9] and that Mg and Be atoms adsorb weakly on graphene[7] (hence the distance between Mg/Be and graphene is large), we conclude that NaC_6-*P6m* possesses the highest superconductivity T_c in all AM and AEM decorated monolayer graphene systems to-date.

Next we lower the M : C concentration to 1 : 8. After the PPSO search, we find that K atoms still distribute uniformly on graphene (with plane symmetry group of *P6m*) due to its large size. However, for NaC_8 and CaC_8, we obtain several structures energetically lower than the uniform pattern. This is consistent with the experimental fact that a regular K (2 × 2) pattern (KC_8) can be realized on graphene surface, while similar uniform CaC_8 does not exist.[34] As shown in Fig. 2a, the ground state of NaC_8 is found in the rectangular supercell and is energetically lower than that of the uniform pattern (Fig. 2b) by 0.133 eV f.u^{-1}. In this structure, the graphene substrate remains flat, and Na atoms adsorb on the quasi-hollow site of C hexagons, forming parallel quasi-1D zigzag chains. This adsorption pattern belongs to the plane symmetry group of *Pmg*. In this NaC_8-*Pmg* structure, the Na–Na relaxed bond length is 3.56 Å, and the vertical distance between the Na chains and the substrate graphene is 2.39 Å. The inter-chain distance between the nearest neighbor chains along the plane of the chains is found to be 7.05 Å, indicating almost negligible interaction between the neighboring chains. In order to examine possible Peierls distortion in the Na chains, we adopted several slightly distorted Na chains as initial structures. Upon re-optimization all systems converged to the same structure shown in Fig. 2a. As for the CaC_8 monolayer, we again find that the ground state adsorption pattern belongs to a rectangle supercell (Fig. 2c), which is favored over the uniform pattern (Fig. 2d) by 0.206 eV f.u^{-1}. Here each unit cell contains five Ca atoms, which are all on the quasi-hollow sites of the graphene substrate. They form a triangular-like flake and are connected together to form several parallel quasi-1D Ca chains. The system belongs to the plane symmetry group of *Pm*. The Ca–Ca bond lengths lie in the range of 3.82–4.00 Å, and the distance between the Ca plane and the graphene sheet is 2.34 Å. Vertical inter-chain distance between the nearest neighbor chains is found to be 5.83 Å.

We calculate the binding energy, E_b, between the metal chains and the graphene substrate using the equation, $E_b = (E_{C_m} + E_{M_n} - E_{M_nC_m})/n$. Here E_{C_m}, E_{M_n} and $E_{M_nC_m}$ are total energies of the graphene, metal chain, and their compound M_nC_m in one unit cell, respectively, and n is the number of metal atoms in one simulating supercell. The calculated E_b for the NaC_8-*Pmg* and the CaC_8-*Pm* are 0.48 and 0.88 eV, respectively. These values confirm the thermodynamic stability of the

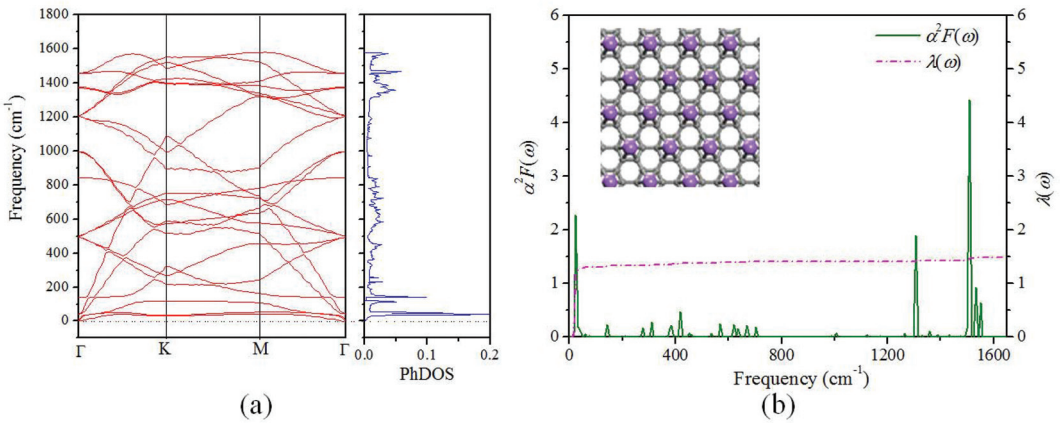

Fig. 1 (a) Phonon dispersion along with phonon density of states and (b) Eliashberg function $\alpha^2F(\omega)$ and electron–phonon coupling parameter $\lambda(\omega)$ of NaC_6-*P6m*. Inset shows the structure of NaC_6-*P6m*.

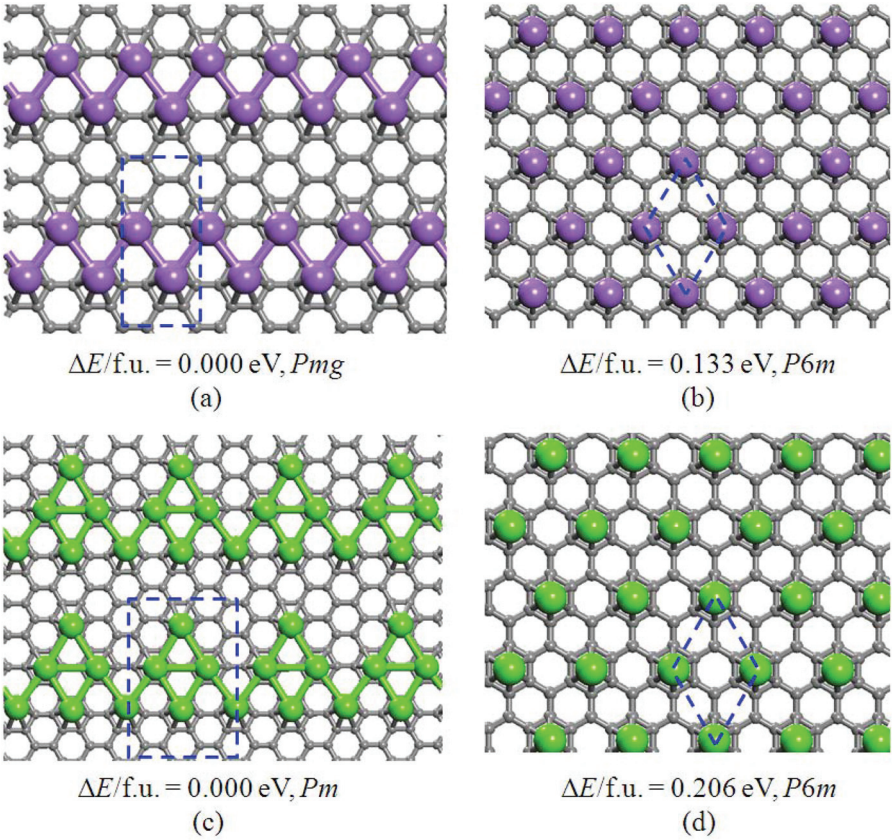

Fig. 2 Ground state structures of (a) NaC_8 and (c) CaC_8, compared with the uniform distribution pattern shown in (b) and (d) respectively. Relative energies per formula unit and plane symmetry groups are shown beneath the structures. Grey, violet, and green spheres represent C, Na, and Ca atoms, respectively. Blue dashed rectangle and rhombus represent unit cells.

adsorbed metal chains on graphene. The thermal stability of the self-assembled Na and Ca chains on the graphene is further investigated by performing *ab initio* molecular dynamics (AIMD) simulations. The Nosé heat bath scheme[35] is used to maintain the temperature at 200 K. We observe that after 5000 steps, with a time step of 1 fs, the structures distort slightly, and the final system can be re-optimized to their stable static structures. This demonstrates that the NaC_8-*Pmg* and the CaC_8-*Pm* are thermally stable at finite temperature.

In order to further confirm the stability of Na and Ca chains on graphene, we calculate the energy barrier necessary to move a single metal atom from the chain along the *y* direction (normal to the chain direction) by using nudged elastic band (NEB) method.[36,37] For the NaC_8-*Pmg*, we use a large rectangular supercell containing Na_6C_{48} to reduce periodic constraints. We find that the energy barrier of moving one Na atom from its original quasi-hollow site to the neighboring quasi-hollow site along the *y* direction is 0.55 eV (Fig. 3a). On the other hand, for the CaC_8-*Pm*, the energy barriers of moving two different in-equivalent Ca atoms from the chain are 0.36 and 0.78 eV, respectively (see Fig. 3b and 3c). These high energy barriers are mainly due to strong metal–metal bond formation energy and indicate that the self-assembled Na and Ca chains are stable at room temperature.

We next calculate the relative energies between the chain-like and uniform distribution pattern when Na and Ca atoms are sandwiched between two graphene layers, forming C_8–Na–C_8 and C_8–Ca–C_8 structures – similar to graphitic intercalation compounds (GIC). We find that for the C_8–Na–C_8, the uniform *P6m* pattern becomes energetically lower than the *Pmg* chain-like pattern by 0.086 eV. On the contrary, the C_8–Ca–C_8 still favors the chain-like pattern rather than the uniform *P6m* by 0.050 eV. We also studied the effect of external electric field on the stability of the NaC_8-*Pmg* and CaC_8-*Pm*. With intermediate electric field, we find that both of the NaC_8-*Pmg* and CaC_8-*Pm* structures are still more stable than their corresponding uniform patterns. For example, for NaC_8, an electric field of 1.0 V $Å^{-1}$ pointing from graphene to Na layer decreases ΔE/f.u. from 133 meV to 41 meV. For CaC_8, the same electric field changes the ΔE/f.u. from 206 meV to 112 meV. These results suggest that the stability of the self-assembled Na and Ca chains on graphene is robust.

We should point out that due to the boundary constraints of the simulating supercells, the self-assembly of Na and Ca chains are found to be parallel to each other. However, due to the six-fold symmetry of the graphene substrate, formation of different atomic chains oriented at 120° with each other is equally probable. Consequently, domain boundaries will exist

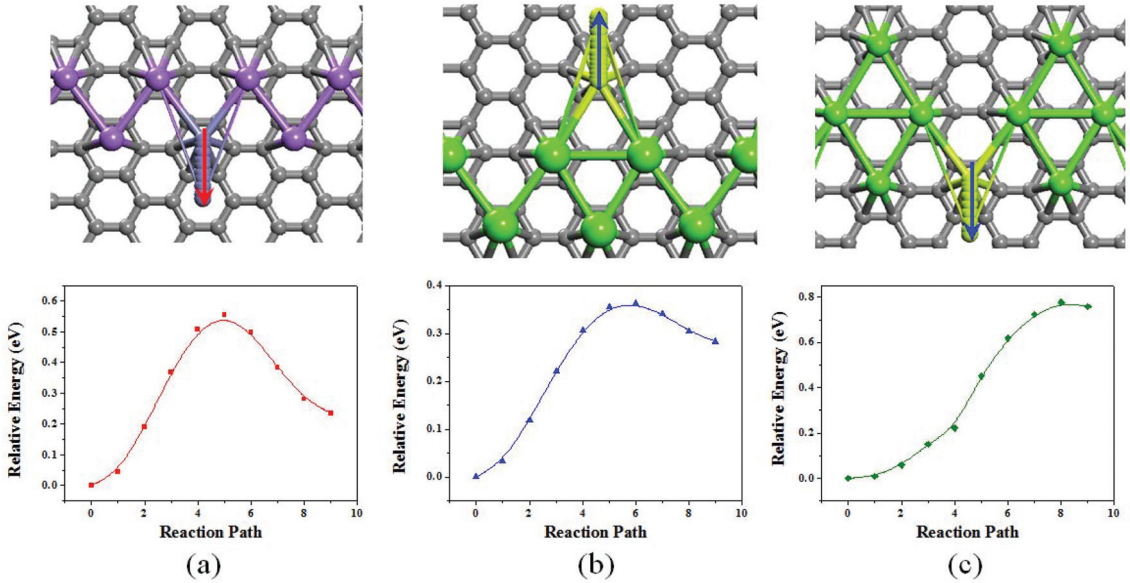

Fig. 3 Sketch of moving a single metal atom (highlighted) from the chain and its corresponding reaction energy profile of (a) NaC_8-*Pmg*, (b) and (c) CaC_8-*Pm*.

to connect these atomic chains. Since this may hinder the self-assembly of parallel metal chains on graphene experimentally, we need to compare the energies between the parallel chain structure and domain boundary connected chain structure. Unfortunately, directly computing the structure containing domain boundaries would require a very large simulating unit cell and is beyond the scope of current computational resource. Therefore, in the following we only provide a qualitative estimate of this possibility. Note that at the domain boundary, the metal (Na or Ca) atoms will form a large cluster. Since no such clustering pattern was found in our PPSO search, it is reasonable to guess that the formation of linear chains is more likely. Hence, we expect that the quasi-1D chains can be seen experimentally without such domain boundaries.

Electron transfer between the metal atoms and the graphene substrate has been examined by calculating their electron density difference $\Delta\rho$ ($= \rho_{M/G} - \rho_G - \rho_M$) where positive and negative values represent electron accumulation and depletion, respectively. In Fig. 4 we plot $\Delta\rho$ of NaC_8-*Pmg* and CaC_8-*Pm*, averaged in the *xy*-plane as well as in slice forms. It can be clearly seen that the Na and Ca atoms transfer electrons to the graphene substrate. By applying Bader's charge analysis[38] we find that on average each Na (Ca) atom donates 0.37 (0.57) electrons to graphene. Thus, graphene is n-doped with carrier concentration of 1.73×10^{14} (2.86×10^{14}) cm^{-2} in NaC_8-*Pmg* (CaC_8-*Pm*).

In Fig. 5a we plot the band structure and the projected density of states (PDOS) of NaC_8-*Pmg* at the GGA-PBE level. We clearly see that the NaC_8-*Pmg* is metallic. The Dirac point of n-doped graphene is located ~1.0 eV below the Fermi level, and opens a small gap of 0.04 eV. We note that for the NaC_8-*P6m* with uniform Na distribution, the position of Dirac point is also ~1.0 eV below the Fermi level, but without any gap

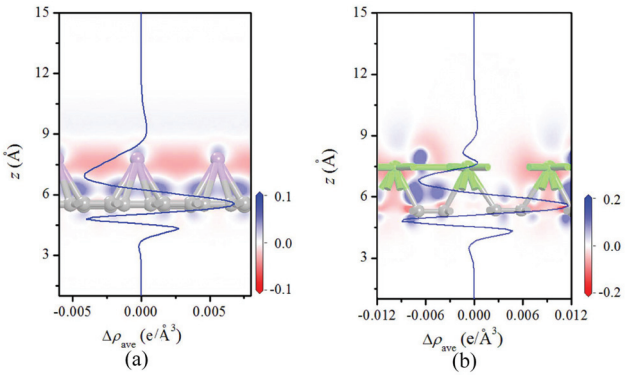

Fig. 4 Electron density difference $\Delta\rho$ averaged in the *xy*-plane and in the 2D slice form of (a) NaC_8-*Pmg* and (b) CaC_8-*Pm*.

opening. From the PDOS, we see that the metallic bands are contributed by both the C and Na atoms. We plot the band decomposed charge densities of two metallic bands (band I and band II) at the Γ point. Note that band I is mainly contributed by the σ orbitals of graphene (Fig. 5b), while band II originates mainly from the Na-s orbitals (Fig. 5c), consistent with the PDOS results. Both of these charge densities are delocalized. Furthermore, in order to see how the Na contributed metallic bands hybridize with the graphene bands, we calculate the relative contribution of Na to each state and map it in the band structure plot using different colors. Red and blue dots represent that the state is contributed only by the C or Na atoms, respectively, while intermediate colors indicate their hybridized states. From Fig. 5a we observe distinct contribution of metallic bands from the C and Na atoms without obvious hybridization. To confirm this, we calculate the band dispersion of the corresponding 'empty' Na (Fig. 5e) and

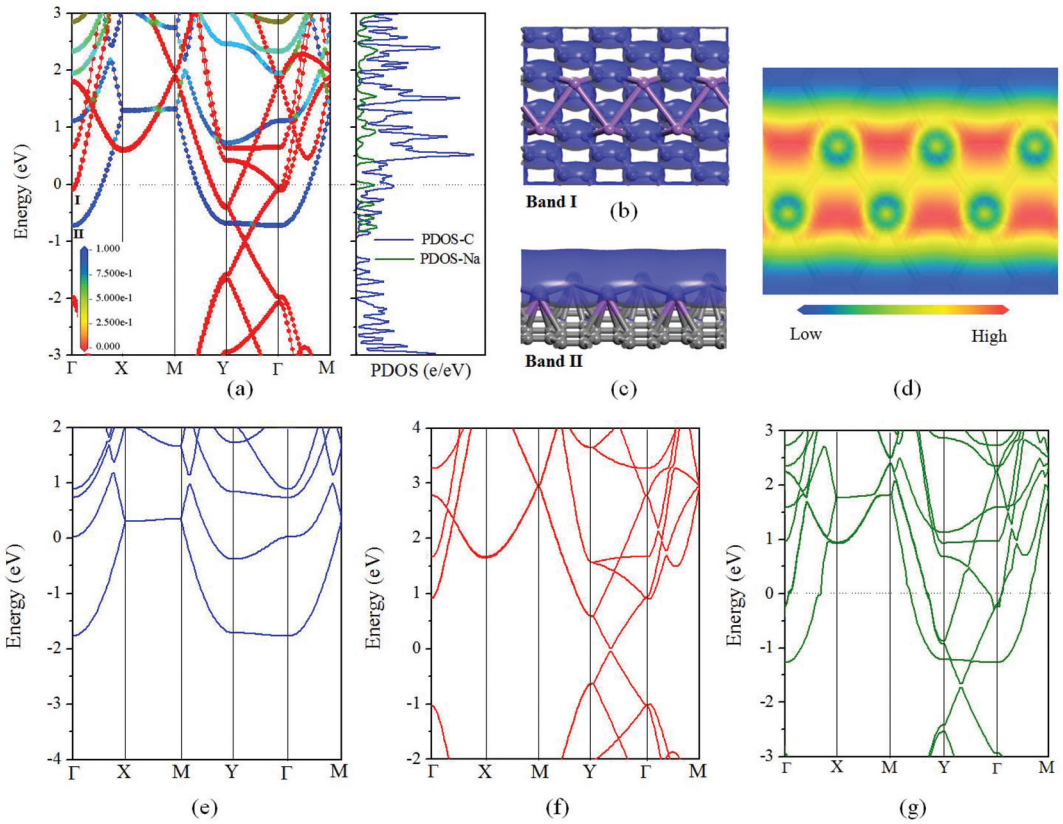

Fig. 5 (a) Band structure and PDOS of NaC_8-*Pmg* at GGA-PBE level. Here Γ (0, 0, 0), X (1/2, 0, 0), M (1/2, 1/2, 0), and Y (0, 1/2, 0) are high symmetry points in the reciprocal space. The Fermi level has been set to zero. In the band structure plot, the relative contribution of Na to the states is illustrated with different colors. Band decomposed charge density of (b) band I and (c) band II at the Γ point (with isosurface value of 0.01 e $Å^{-3}$). (d) Simulated STM image under −2 V bias voltage. Band structure dispersions of (e) 'empty' Na and (f) 'empty' graphene. (g) Band structure of the NaC_8-*Pmg* calculated at HSE06 level.

'empty' graphene (Fig. 5f), which can be obtained by removing the C and Na atoms from the NaC_8-*Pmg*, respectively, while keeping the lattice constants and the remaining atomic positions fixed. The band dispersions of the NaC_8-*Pmg* around the Fermi energy resemble the combination of the 'empty' graphene and 'empty' Na dispersions, along with relative energy shifted due to electron transfer between them. This "rigid band" character is different from those in previously reported AM deposited graphene systems.[5,6] These results demonstrate that the Na atomic chain on graphene can retain its electronic property similar to that of its isolated state, thus it can mimic the 1D electron Luttinger liquid state. Due to the high chemical reactivity, Na atoms cannot form freestanding quasi-1D extended systems (see Fig. S1 in ESI†); hence, our results suggest a viable strategy to stabilize Na atomic chains without perturbing its band structure. In addition, we observe that the Na contributed bands are nearly flat along the *y* direction (X → M and Y → Γ paths), which demonstrates that the interaction between two chains is negligible. The calculations were repeated by applying hybrid functional proposed by Heyd, Scuseria, and Ernzerhof (HSE06)[39,40] which is believed to describe the exchange correlation energy more accurately. As shown in Fig. 5g, the difference between the HSE06 and the GGA-PBE lies only in the energy level shift away from the Fermi level (*e.g.* the Dirac point of graphene moves to 1.7 eV below the Fermi level and opens a gap of 0.07 eV), but the dispersion profiles remain unchanged. The Na and graphene contributed metallic bands are still distinct from each other, without any obvious hybridization. Due to computational cost, it is not possible to calculate EPC of the NaC_8-*Pmg* and estimate its possible T_c directly. However, considering that lower metal coverage on graphene leads to smaller EPC, we expect that the possible superconducting T_c of the NaC_8-*Pmg* is smaller than that of the NaC_6-*P6m*. To provide more information for future experiments and manipulation of such novel well-aligned metal chains at atomic scale, we simulated constant-current scanning tunneling microscope (STM) image of the system (Fig. 5d).[41] Here the bright sites appear around the Na chains.

In Fig. 6 we plot the energy band structure and electron density of states of CaC_8-*Pm*. From the band structure (Fig. 6a) we see that the CaC_8-*Pm* is also metallic. The Dirac point of this functionalized graphene lies 1.3 eV below the Fermi level and opens a small gap of 0.03 eV. Calculations show that no Dirac point gap opening exists in the uniformly decorated CaC_8-*P6m* system. By using the HSE06 hybrid functional (Fig. 6b) we confirm the band profile and the metallicity obtained at the GGA-PBE level. In order to analyze the metallic

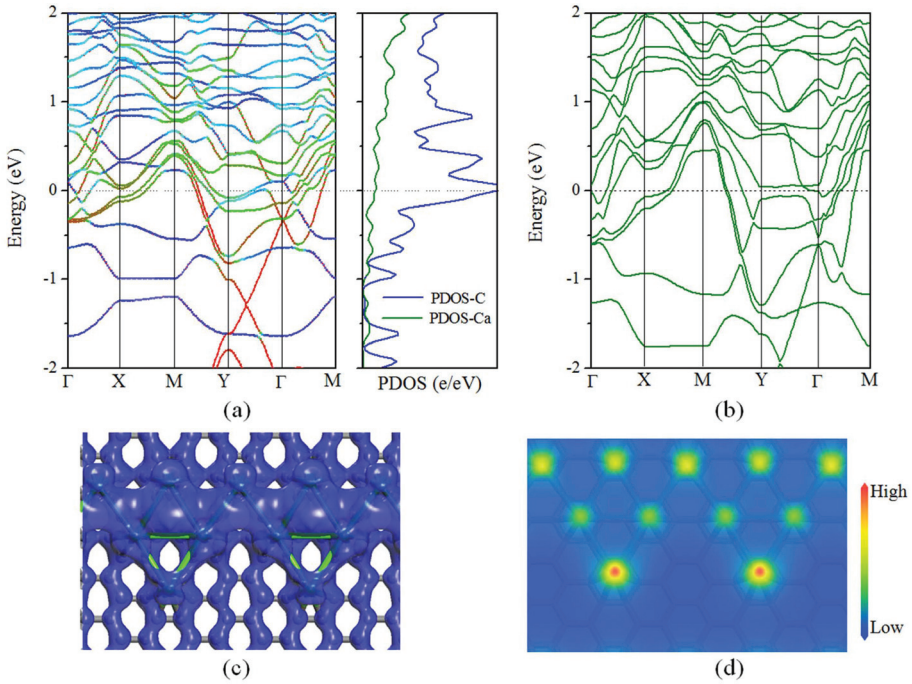

Fig. 6 (a) Band structure and PDOS of CaC_8-*Pm* at GGA-PBE level, with relative Ca contribution shown in different colors (color bar is the same as in Fig. 4a). (b) Band structure calculated by HSE06 hybrid functional. (c) Band decomposed electron density of states near the Fermi energy. (d) Simulated STM adatoms image under bias voltage of −2 V.

bands, we first plot the band decomposed charge density of the states around the Fermi level (Fig. 6c) as well as the relative contribution of Ca in all the states. In contrast to NaC_8-*Pmg*, we find that most states of the metallic bands are contributed by both C and Ca atoms, and no bands can be associated with solely Ca chains. In order to further see whether the electronic property of Ca chain on graphene is similar to that of its isolated state, we calculate the band structure of 'empty' Ca chain with the graphene removed from the system (see Fig. S2 in the ESI†). It is difficult to identify the correspondence between any metallic bands of the CaC_8-*Pm* and the bands of 'empty' Ca chain. These results indicate that, in addition to the charge transfer, significant hybridization also exists between the graphene substrate and the Ca chain. Thus, it is difficult to study and examine the electronic properties of only Ca chain without the influence of the graphene substrate. In Fig. 6d we plot the simulated STM image of the CaC_8-*Pm* system, which clearly shows that Ca sites correspond to bright sites.

One important property of a metallic surface is its work function (WF) which measures the energy required to remove one electron. It is calculated as the difference between the electrostatic potential energy in the vacuum ($-e\Phi$) and the Fermi energy (E_F), *i.e.* WF = $-e\Phi - E_F$. We assess the effects of different metal adsorptions on the WFs at various concentrations (MC_x with $x = \infty$, 32, 8, and 6), where the optimal structures of MC_6 and MC_8 are obtained from our PPSO search, and the MC_{32} is simulated by adsorbing one M atom on a (4 × 4) graphene supercell. As for pure graphene, its WF is calculated to be 4.48 eV, in agreement with previous calculations.[42] When metal atoms are introduced, we find that the WF values are decreased (see Fig. S3 in ESI†). The WFs of NaC_{32}, KC_{32}, and CaC_{32} are 3.36, 3.35, and 3.45 eV, respectively, and their values further reduce as metal concentrations increase. It can be observed that generally $WF_{KC_x} < WF_{NaC_x} < WF_{CaC_x}$ for each x, which agrees with the trend in their corresponding ionization potential energies, K (4.34 eV) < Na (5.14 eV) < Ca (6.11 eV).[43]

IV. Conclusion

In summary, by using PPSO algorithm we performed a thorough search of the adsorption pattern of Na, Ca, and K on graphene surface. We find that when the coverage ratio M : C exceeds 1 : 6, all the three metal atoms are distributed uniformly. Among these systems, NaC_6 is a BCS superconductor and has the highest critical temperature, T_c = 5.8 K of any known stable alkali or alkaline-earth metal decorated graphene. When the M : C ratio decreases to 1 : 8, K atoms still prefer uniform distribution, while the Na and Ca atoms form stable self-assembled quasi-1D metallic chains. Except for electron transfer, the Na chain has marginal hybridization with the graphene substrate, and possesses the electronic property similar to that of its isolated state. We also find that high coverage of metals on graphene decreases the work function of the system. This study highlights the effect of different metal species and their concentration on the distribution pattern on

graphene and emphasizes the underlying structure–property relationships.

Acknowledgements

This work is partially supported by grants from the U.S. Department of Energy, Office of Basic Energy Sciences, Division of Materials Sciences and Engineering under Award # DE-FG02-96ER45579 and the National Grand Fundamental Research 973 Program of China (2012CB921404). The authors thank the crew of the Center for Computational Materials Science, the Institute for Materials Research, Tohoku University (Japan), for their continuous support of the HITACHSR11000 supercomputing facility.

References

1 K. S. Novoselov, A. K. Geim, S. V. Morozov, D. Jiang, Y. Zhang, S. V. Dubonos, I. V. Grigorieva and A. A. Firsov, *Science*, 2004, **306**, 666.
2 J. O. Sofo, A. S. Chaudhari and G. D. Barber, *Phys. Rev. B: Condens. Matter*, 2007, **75**, 153401.
3 H. J. Xiang, S.-H. Wei and X. G. Gong, *Phys. Rev. B: Condens. Matter*, 2010, **82**, 035416.
4 J. Zhou, M. Wu, X. Zhou and Q. Sun, *Appl. Phys. Lett.*, 2009, **95**, 103108.
5 G. Profeta, M. Calandra and F. Mauri, *Nat. Phys.*, 2012, **8**, 131.
6 K.-H. Jin, S.-M. Choi and S.-H. Jhi, *Phys. Rev. B: Condens. Matter*, 2010, **82**, 033414.
7 S.-M. Choi and S.-H. Jhi, *Phys. Rev. Lett.*, 2008, **101**, 266105.
8 Y. Liu, Y. M. Wang, B. I. Yakobson and B. C. Wood, *Phys. Rev. Lett.*, 2014, **113**, 028304.
9 M. Liu, A. Kutana, Y. Liu and B. I. Yakobson, *J. Phys. Chem. Lett.*, 2014, **5**, 1225.
10 N. Oncel, *J. Phys.: Condens. Matter*, 2008, **20**, 393001.
11 J. K. Bera and K. R. Dunbar, *Angew. Chem., Int. Ed.*, 2002, **41**, 4453.
12 J. Voit, *Rep. Prog. Phys.*, 1994, **58**, 977.
13 C. Blumenstein, J. Schäfer, S. Mietke, S. Meyer, A. Dollinger, M. Lochner, X. Y. Cui, L. Patthey, R. Matzdorf and R. Claessen, *Nat. Phys.*, 2011, **7**, 776.
14 T. Aruga, H. Tochihara and Y. Murata, *Phys. Rev. Lett.*, 1984, **53**, 372.
15 L. Gavioli, M. Padovani, E. Spiller, M. Sancrotti and M. G. Betti, *Appl. Surf. Sci.*, 2003, **212**, 47.
16 A. Calzolari, C. A. Pignedoli, R. Di Felice, C. M. Bertoni and A. Catellani, *Surf. Sci.*, 2001, **491**, 265.
17 I. N. Yakovkin, *Appl. Surf. Sci.*, 2006, **252**, 6127.
18 J. P. Perdew, K. Burke and M. Ernzerhof, *Phys. Rev. Lett.*, 1996, **77**, 3865.
19 G. Kresse and J. Furthmuller, *Phys. Rev. B: Condens. Matter*, 1996, **54**, 11169.
20 G. Kresse and J. Joubert, *Phys. Rev. B: Condens. Matter*, 1999, **59**, 1758.
21 H. J. Monkhorst and J. D. Pack, *Phys. Rev. B: Solid State*, 1976, **13**, 5188.
22 S. Grimme, *J. Comput. Chem.*, 2006, **27**, 1787.
23 P. Giannozzi, S. Baroni, N. Bonini, M. Calandra, R. Car, C. Cavazzoni, D. Ceresoli, G. L. Chiarotti, M. Cococcioni, I. Dabo, A. D. Corso, S. de Gironcoli, S. Fabris, G. Fratesi, R. Gebauer, U. Gerstmann, C. Gougoussis, A. Kokalj, M. Lazzeri, L. Martin-Samos, N. Marzari, F. Mauri, R. Mazzarello, S. Paolini, A. Pasquarello, L. Paulatto, C. Sbraccia, S. Scandolo, G. Sclauzero, A. P. Seitsonen, A. Smogunov, P. Umari and R. M. Wentzcovitch, *J. Phys.: Condens. Matter*, 2009, **21**, 395502.
24 S. Baroni, S. de Gironcoli, A. Dal Corso and P. Giannozzi, *Rev. Mod. Phys.*, 2001, **73**, 515.
25 Y. Wang, J. Lv, L. Zhu and Y. Ma, *Phys. Rev. B: Condens. Matter*, 2010, **82**, 094116.
26 J. Lv, Y. Wang, L. Zhu and Y. Ma, *J. Chem. Phys.*, 2012, **137**, 084104.
27 Y. Wang, M. Miao, J. Lv, L. Zhu, K. Yin, H. Liu and Y. Ma, *J. Chem. Phys.*, 2012, **137**, 224108.
28 L. Zhu, Z. Wang, Y. Wang, G. Zou, H.-k. Mao and Y. Ma, *Proc. Natl. Acad. Sci. U. S. A.*, 2012, **109**, 751.
29 S. Lu, Y. Wang, H. Liu, M.-s. Miao and Y. Ma, *Nat. Commun.*, 2014, **5**, 3666.
30 R. Eberhart and J. Kennedy, *A New Optimizer Using Particle Swarm Theory*, IEEE, New York, NY, 1995.
31 E. Clementi, D. L. Raimond and W. P. Reinhardt, *J. Chem. Phys.*, 1967, **47**, 1300.
32 W. L. McMillan, *Phys. Rev.*, 1967, **167**, 331.
33 P. B. Allen and R. Dynes, *Phys. Rev. B: Solid State*, 1975, **12**, 905.
34 J. L. McChesney, A. Bostwick, T. Ohta, T. Seyller, K. Horn, J. Gonzalez and E. Rotenberg, *Phys. Rev. Lett.*, 2010, **104**, 136803.
35 S. Nosé, *J. Chem. Phys.*, 1984, **81**, 511.
36 G. Henkelman, B. P. Uberuaga and H. Jónsson, *J. Chem. Phys.*, 2000, **113**, 9901.
37 G. Henkelman and H. Jónsson, *J. Chem. Phys.*, 2000, **113**, 9978.
38 W. Tang, E. Sanville and G. Henkelman, *J. Phys.: Condens. Matter*, 2009, **21**, 084204.
39 J. Heyd, G. E. Scuseria and M. Ernzerhof, *J. Chem. Phys.*, 2003, **118**, 8207.
40 J. Heyd, G. E. Scuseria and M. Ernzerhof, *J. Chem. Phys.*, 2006, **124**, 219906.
41 J. Tersoff and D. R. Hamann, *Phys. Rev. B: Condens. Matter*, 1985, **31**, 85.
42 G. Giovannetti, P. A. Khomyakov, G. Brocks, V. M. Karpan, J. van den Brink and P. J. Kelly, *Phys. Rev. Lett.*, 2008, **101**, 026803.
43 J. A. Dean, *Lange's handbook of chemistry*, McGraw-Hill, New York, 15th edn, 1999.